it is possible for a transition involving an s-state core level to have a divergent threshold behavior for APS and not for the x-ray case.

In conclusion we note that many simplifying physical assumptions are embodied in the model Hamiltonian and just as in the x-ray case,[7] additional effects may tend to smear the threshold behavior. However, the contrasts between APS and x-ray threshold behavior hopefully will encourage experimental tests of the predictions of the model.

I would like to thank L. Dworin for a critical reading of this manuscript and I am grateful to P. Nozières and to D. C. Langreth for calling Ref. 20 to my attention.

*Work supported by the U. S. Atomic Energy Commission.

[1]R. Haensel, C. Keitel, P. Schreiber, B. Sonntag, and C. Kunz, Phys. Rev. Lett. 23, 528 (1969).
[2]F. C. Brown, C. Gähwiller, A. B. Kunz, and N. O. Lipari, Phys. Rev. Lett. 25, 927 (1970).
[3]C. Gähwiller and F. C. Brown, Phys. Rev. B 2, 1918 (1970).
[4]G. D. Mahan, Phys. Rev. 163, 612 (1967).
[5]B. Roulet, J. Gavoret, and P. Nozières, Phys. Rev. 178, 1072 (1969).
[6]P. Nozières, J. Gavoret, and B. Roulet, Phys. Rev. 178, 1084 (1969).
[7]P. Nozières and C. T. De Dominicis, Phys. Rev. 178, 1097 (1969).
[8]K. D. Schotte and U. Schotte, Phys. Rev. 182, 479 (1969).
[9]D. C. Langreth, Phys. Rev. 182, 973 (1969).
[10]G. A. Ausman and A. Glick, Phys. Rev. 183, 687 (1969).
[11]J. J. Hopfield, Comments Solid State Phys. 2, 40 (1969).
[12]R. L. Park, J. E. Houston, and D. G. Schreiner, Rev. Sci. Instrum. 41, 1810 (1970).
[13]J. E. Houston and R. L. Park, J. Vac. Sci. Technol. 8, 91 (1971).
[14]D. C. Langreth, Phys. Rev. Lett. 26, 1229 (1971).
[15]G. E. Laramore, unpublished.
[16]See L. Van Hove, Phys. Rev. 95, 249 (1954), for a discussion of the correlation-function approach to the scattering problem in solids.
[17]A. L. Fetter and J. D. Walecka, *Quantum Theory of Many-Particle Systems* (McGraw-Hill, New York, 1971), Chap. 3.
[18]N. I. Muskhelishvili, *Singular Integral Equations*, translated by J. R. M. Radok (P. Noordhoff N.V., Groningen, The Netherlands, 1953), Chap. 14.
[19]Note that because the electrons are fermions, $W(\vec{k}_4, \vec{k}_1, \vec{k}_2) = -W(\vec{k}_4, \vec{k}_2, \vec{k}_1)$ and so the two terms in Eq. (19) add instead of canceling.
[20]M. Natta and P. Joyes, J. Phys. Chem. Solids 31, 447 (1970).

Direct Evidence for Disorder Effects on the Electronic Structure of Selenium

L. D. Laude and B. Fitton
Surface Physics Division, European Space Research Organization, Noordwijk, Holland

and

B. Kramer and K. Maschke
Institut für Theoretische Physik (II) der Universität Marburg, Marburg, Germany

(Received 4 June 1971)

The electron states of amorphous and single-crystal trigonal selenium were investigated by high-resolution photoemission spectroscopy. Structures due to a high density of states 0.2 eV below and 6.9 eV above the valence-band edge for crystalline Se are absent in the amorphous phase, but structures due to deeper valence-band density-of-states features remain. The results provide the first direct evidence for disorder effects on the Se valence and conduction bands and agree with calculations for amorphous Se using a pseudopotential formalism.

There have been a number of band-structure calculations for trigonal selenium, the most recent due to Sandrock[1] using the pseudopotential method. A pseudopotential formalism was also adopted recently by Kramer and co-workers[2-4] in their approach to the problem of calculating

the electron states of the amorphous phase of selenium. In all of these studies calculations were made of the imaginary part ϵ_2 of the dielectric constant, and a comparison was made with the optically determined spectrum of ϵ_2.[5] The agreement has been good in the case of the pseudopotential calculations for both the trigonal and the amorphous phase. The disadvantage of using ϵ_2 experimental determinations for a comparison with theoretical calculations is, of course, the inherent uncertainty which lies in assigning the observed transition energies relative to the valence-band edge. This problem is overcome by using the photoemission technique which is particularly attractive when attempting to compare the changes in energy levels which accompany the transformation from the crystalline to the disordered state.

It is difficult to assign accurately the peaks in the photoelectron energy distributions resulting from high density of states (DOS) to particular regions in $\vec{k}$ space from the band structure alone because of the rather flat bands of selenium. Therefore it is desirable to calculate the DOS itself. This calculation has already been performed for crystalline Se,[6] including contributions from different regions in the Brillouin zone [Fig. 1(a)]. For amorphous Se we can use the following equation[4]:

$$n_{\mathrm{amorph}}(E) \sim \sum_m \int d^3k \, \mathrm{Im}[E - \epsilon_m(\vec{k})]^{-1},$$

where $\epsilon_m(\vec{k}) = E_m(\vec{k}) + i\Gamma_m(\vec{k})$ denotes the complex energy appearing in the complex band structure of the amorphous phase.[3] The real part of the energy is approximately the same as for crystalline Se. The imaginary part of the energy is nearly independent of $\vec{k}$. Therefore we can perform the calculation by lifetime-broadening of the crystal contributions to the DOS using averaged imaginary parts of the energy. The result is shown in Fig. 1(b). We notice that certain sharp structures in the DOS are smoothed out in the amorphous case.

The experimental techniques used in this study of the second derivative of the photoelectron energy distribution curves (EDC's) have been discussed elsewhere.[7] With these techniques the resolution is improved by a factor of approximately 5 compared with conventional EDC measurements[8] using, for instance, a 0.3-V modulation amplitude in both cases. Throughout the actual measurements the energy resolution was between 50 and 150 meV. The results for trigonal selenium were obtained from the $(10\bar{1}0)$ face of single crystals. Cleaving was carried out in a vacuum of 5×10^{-11} Torr using the arrangement described earlier.[9] The amorphous films were evaporated onto flame-polished silica substrates provided with silver side contacts to the copper holder. They were typically 500 Å thick and exhibited a red transparency. The sample was inserted into the same gold-coated spherical analyzer as used for trigonal Se, the vacuum being 1×10^{-10} Torr during and after evaporation. The photoelectric threshold for the $(10\bar{1}0)$ face of selenium was determined to be 5.9 ± 0.1 eV. Since the width of the first conduc-

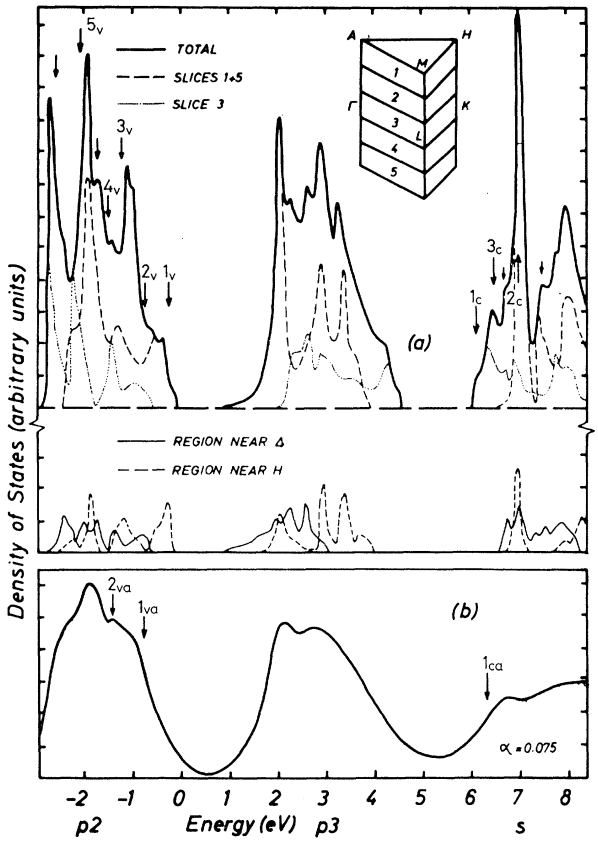

FIG. 1. Density of states of Se. (a) Crystalline case, total DOS and contributions from different $\vec{k}$ regions; (b) amorphous case, calculated by using the imaginary parts of energy from Ref. 3. The comparison with the crystalline DOS and the complex band structure shows that the vanishing of peaks 1_v and 2_c is due to relatively large imaginary parts of energy in the respective $\vec{k}$ regions. The large arrows denote the positions of structures observed in the photoemission spectra (see Fig. 2). The small arrows refer to weak structures in the s-like upper conduction band, which can be related to two substructures at $\mathcal{E} = 6.7$ and 7.4 eV occurring in the range $h\nu = 7.3$–8.0 eV in Fig. 2.

tion-band triplet (p_3) in trigonal selenium is about 3 eV, with the minimum being located about H, some eV above the top of the valence band,[1] it follows that no details of the p_3 band can be obtained from a photoemission investigation.

The structures obtained in the second derivative of the photoelectron energy distribution from crystalline selenium are given in Fig. 2 as a function of photon energy between 6.3 and 8.9 eV. The experimental yield of the samples used was found to be small, of the order of 10^{-4} electrons per absorbed photon at 8 eV, for unpolarized light. Further reduction of the yield was imposed by the polarizer, which limited the measurements with polarized light to the energy range 7.2–8.1 eV. Over that energy range, the spectra exhibited a number of polarization-dependent fine structures whose intensity varied sharply with energy and which lay within the main structures that are described by strong DOS features in either the conduction or the valence band. The behavior of these fine structures is consistent with DOS features which are well localized in $\vec{k}$ space [Fig. 1(a)]. The structures that lie on curves about the 45° axis in Fig. 2 may be assigned to high DOS in the valence band and read as initial-state energies ($\mathcal{E} - h\nu$), where the energy zero is taken as the top of the valence band. Structures which move across the diagram along complex curves are typical of direct transitions in which features in the joint density of initial and final states are operative. In addition, indirect processes together with relaxation can lead to dominant structures in the electron energy distribution, which provide specific information on the location of high conduction-band DOS.

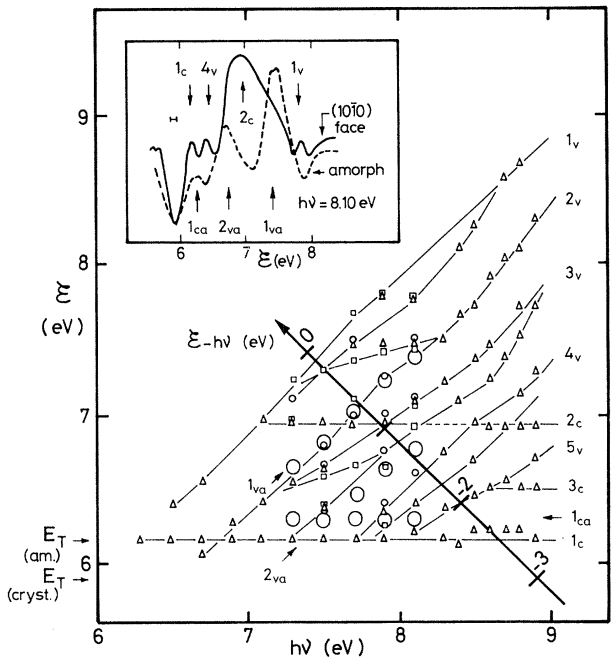

FIG. 2. Energy diagram of structures appearing in the photocurrent third harmonic for trigonal Se (triangles, no polarization; small circles, $\vec{E} \parallel \vec{c}$; squares, $\vec{E} \perp \vec{c}$) and for amorphous Se (large circles) as a function of photon energy. Final-state energy levels $\mathcal{E}$ refer to the valence-band edge. Valence-band DOS structures are also referred to the valence-band edge (where $\mathcal{E} - h\nu = 0$) on the 45° axis across the diagram. In the insert are shown two spectra obtained at $h\nu = 8.1$ eV from a trigonal Se (10$\bar{1}$0) face (solid line) and from an amorphous Se film (dashed line). Between 7.3 and 8.0 eV the oscillator strength remains nearly constant (see Ref. 5), in which case the joint density of states can be considered to account for the branching of 1_v to 2_v and 2_v to 3_v in that energy range (see Fig. 1 caption).

We shall discuss first the crystalline case. The structure labeled 1_c, stable at 6.15 eV, is present in all of the traces obtained and is not strongly polarization sensitive. This structure can be assigned to the low-energy edge of the DOS of the second conduction band, which mainly contains contributions from states near K and L. The structure 1_v appears at $h\nu = 6.5$ eV. It persists throughout the measurements and moves according to the increase in photon energy. It occurs mainly for $\vec{E} \perp \vec{c}$ and is centered some −0.2 eV below the valence-band edge. Transitions from a region around H are responsible for the upper section of 1_v close to the valence-band edge, between 0 and −0.2 eV, while the rest of the top plane in the Brillouin zone contributes to the extension of 1_v down to about −0.5 eV. This assignment explains both the strong polarization dependence of 1_v for points very close to the valence-band edge (in agreement with selection rules[1] about H) and its rather small relative intensity.

At about $h\nu = 7.2$ eV, a strong structure 2_c begins which remains stable at $\mathcal{E} = 6.9$ eV, increasing rapidly in strength up to $h\nu = 8.0$ eV. We note that in the DOS spectrum of Fig. 1(a), a very sharp peak is present at 7.1 eV, which can essentially be assigned to the top plane of the Brillouin zone. If, in addition, we note that 2_c starts very close to 1_v at 0.1 or 0.2 eV below the valence-band edge (i.e., from initial states about the top of p_2 at H), we may conclude that 2_c corresponds to the low-energy edge of this large peak in the conduction band DOS. For photon en-

ergies between 7.0 and 7.2 eV, the transitions are direct between the top of p_2 and the bottom of the second conduction band about H, then become indirect on increasing $h\nu$, with initial states lying as low as −1.3 eV (L point in Sandrock's notation). Structures 2_v and 3_v, although well separated at low energies, tend to mix and extend from −0.5 to −1.0 eV. A comparison with Fig. 1(a) shows that 2_v can be assigned to transitions in slice 3. The structure 3_v is due to transitions occurring mainly in slices 2 and 4 of the Brillouin zone. In the ϵ_2 spectra, a strong peak observed between 7.5 and 8.0 eV was attributed to transitions between p_2 and the lowest sub-band of the second conduction band.[10] This structure is due to a strong anisotropic-oscillator strength mostly near the $k_z=0$ plane, with transitions at K only allowed for $\vec{E}\parallel\vec{c}$. The photoemission spectra do exhibit polarization dependence between 7.5 and 7.9 eV, with a strong $\vec{E}\parallel\vec{c}$ substructure localized 0.7 eV below the valence-band edge. This detail supports both Sandrock's interpretation of ϵ_2 spectra and the proposed 2_v assignment. Deeper in the valence band, two other structures, 4_v and 5_v, appear at nearly −1.6 and −2.1 eV, respectively. In addition, 2_c reappears when electrons are being excited from 4_v, at $h\nu=8.5$ eV. From Fig. 1(a) we conclude that 4_v is contributed by transitions along Δ and slice 3 [Fig. 1(a)], and 5_v by transitions from the whole Brillouin zone. The structure 5_v stabilizes into 3_c for $h\nu=8.7$ eV at $\mathcal{E}=6.5$ eV. It corresponds to a high density of states in the s conduction band, as pointed out in Fig. 1. Additional data were obtained up to 11 eV. A new structure appears around $h\nu=9.2$ eV and remains stable at −2.5 eV, indicating the bottom of p_2. It corresponds to a peak in Fig. 1(a) at −2.6 eV. Transitions initiated at the top of p_1 start at $h\nu=9.6$ eV and result in a strong peak in our data at −3.4 eV in agreement with other work[8] and the actual DOS of Maschke and Thomas.[11]

Second-derivative spectra of electron energy distribution curves were obtained from amorphous Se layers in the range 7.3 to 8.1 eV, the extent of this range being limited by the very low yield found for these films, which was two orders of magnitude lower than for trigonal Se. As shown in the insert of Fig. 2, the amorphous and crystalline Se obtained at 8.1 eV reveal a strong difference. Two peaks, labeled 1_{va} and 2_{va}, in the amorphous Se spectra stand around −0.7 and −1.4 eV, respectively. They correspond to peaks at nearly −0.9 and −1.4 eV, respectively, in Fig. 1(b). These two are essentially caused by the preservation of the Δ contribution to the DOS (small imaginary parts) when going from the crystalline to the amorphous structure. On the other hand, structure 2_c has disappeared totally, in agreement with the computed amorphous Se DOS. The next interesting point is that the structure 1_v does not show up for amorphous Se, at least not as a well-resolved structure. Instead, the high-energy edge of these spectra consists of a smooth ramp, probably extending slightly over the valence-band edge as located in crystalline Se. This might be interpreted in terms of a DOS tailing the p_2-p_3 band gap, but no definite conclusions can be drawn on this point from these measurements since the energy resolution, 150 meV in this case, is probably of the same order of magnitude as the tailing of the DOS in amorphous Se. The low-energy edge of the amorphous Se spectra remains stable and results in the structure 1_{ca} at $\mathcal{E}=6.3$ eV (photoelectric threshold was found to be 6.15 eV for amorphous Se). This structure results from a mixing of contributions from all sections of the Brillouin zone and corresponds to a shoulder in the DOS as shown in Fig. 1(b). The additional structures at −2.0 and −2.5 eV, predicted to persist in the amorphous Se spectra, appear above $h\nu=8$ eV and therefore were not detected within the photon energy range used for amorphous Se. All three structures observed in amorphous Se spectra can be considered as confirming theoretical estimates. These measurements show very clearly the effects of disorder in the conduction- and valence-band DOS of selenium.

Two of us (L.D.L. and B.F.) thank Dr. E. A. Trendelenburg for his encouragement and gratefully acknowledge the excellent assistance of M. Barnes.

This paper resulted from a collaboration initiated at the Europhysics Conference on the Physics of Se and Te, May 1971, for which we thank Professor J. Stuke and Professor M. Hulin.

[1]R. Sandrock, Phys. Rev. 169, 642 (1968).

[2]B. Kramer, K. Maschke, P. Thomas, and J. Treusch, Phys. Rev. Lett. 25, 1020 (1970).

[3]B. Kramer, Phys. Status Solidi 41, 725 (1970).

[4]B. Kramer, Phys. Status Solidi 41, 649 (1970).

[5]S. Tutihasi, G. G. Roberts, R. C. Keezer, and R. E. Drews, Phys. Rev. 177, 1143 (1969); M. Cardona, W. Gudat, B. Sonntag, and P. Y. Yu, in *Proceedings of the Tenth International Conference on the Physics of Semiconductors, Cambridge, Mass., 1970,* edited by

S. P. Keller, J. C. Hensel, and F. Stern, CONF-700801 (U. S. AEC Division of Technical Information, Springfield, Va., 1970); J. Stuke, in *Advances in Solid State Physics. Festkörperprobleme IX*, edited by O. Madelung (Pergamon, New York, 1969).

[6]K. Maschke, Ph.D. thesis, University of Marburg, 1970 (unpublished).

[7]L. D. Laude, B. Fitton, and M. Anderegg, Phys. Rev. Lett. 26, 637 (1971).

[8]P. Nielsen, Bull. Amer. Phys. Soc. 16, 349 (1971).

[9]M. R. Barnes and L. D. Laude, to be published.

[10]R. Sandrock, Phys. Status Solidi (b) 43, 199 (1971).

[11]K. Maschke and P. Thomas, Phys. Status Solidi 41, 743 (1970).

Surface Plasmons and the Reflectivity of *n*-Type InSb†

William E. Anderson and Ralph W. Alexander, Jr.
Physics Department, University of Missouri—Rolla, Rolla, Missouri 65401

and

Robert J. Bell
Physics Department and Graduate Center for Materials Research, University of Missouri—Rolla, Rolla, Missouri 65401

(Received 30 June 1971)

The reflectivity of *n*-type InSb has been measured in the far infrared. The doping of the samples was such that the free-carrier plasma frequency was near the LO mode frequency. The results suggest that samples with a sufficiently thick damage layer show effects due to surface plasmons. Use of a simple model indicates that the surface-plasma excitations are coupled to the phonons.

Surface-plasma excitations were observed by Wood[1] but were not understood until much later. The phenomenon of "Wood's anomalies" was then used by Ritchie to study surface plasmons in Al and Au.[2] Energy loss to surface plasmons by high-energy electrons has been observed for a number of thin metal films. More recently, enhanced photoemission from metals due to surface plasmons has been observed by Spicer and coworkers.[3] Tsui[4] has also observed the interaction of tunneling electrons with surface plasmons in degenerate *n*-type GaAs. Ngai, Economou, and Cohen[5] have provided a theoretical interpretation of Tsui's measurements.

For metals, the surface-plasmon frequency is in the visible, while for degenerate semiconductors this frequency is in the infrared. For example, the surface-plasma frequency for the GaAs samples of Tsui was about 800 cm^{-1} (100 meV), considerably above the phonon frequencies in that material. We report reflectivity measurements for Te-doped InSb samples with surface-plasmon frequencies in the 200-cm^{-1} range. Thus, the surface-plasmon frequencies lie near the longitudinal optical-phonon frequencies. This considerably complicates the problem since coupling between the surface plasmons and the optical phonons is now possible. Our data, in fact, show that such coupling is important. We shall use a very simple model in which retardation effects are neglected to explain qualitatively our observations. Of course, retardation effects will be important for the relatively small wave vectors used in our experiments, and a more complete interpretation awaits a theory including the surface-plasmon–optical-phonon coupling and retardation.

The InSb samples were Te doped. Reflectivity measurements were made with three different impurity concentrations such that the free-carrier plasma frequency was in the range 160 to 269 cm^{-1}. The plasma frequency ω_p is related to the free-carrier concentration by

$$\omega_p^2 = 4\pi Ne^2/m^*\epsilon_\infty. \quad (1)$$

The $\vec{k}=0$ longitudinal optical phonon of InSb is approximately 190 cm^{-1}. A commercial far-infrared Michelson interferometer was used with which the angle of incidence and the polarization of the incident beam could be varied.

Clean, optically polished samples gave results in substantial agreement with published reflectivities.[6] In an attempt to adapt the method used by Ritchie[2] for metals, a grating of 80 lines per cm was cut on all the grating samples. The grating profile was semicircular with 63.5-μm-diam grooves separated by 63.5-μm uncut strips (see inset on Fig. 1). A spark cutter was used